

## Dynamic electrochemical assessment of redox reactions in natural micas between 613 and 1373 K at $10^5$ Pa

DOROTHEE J.M. BURKHARD,<sup>1,\*</sup> GENE C. ULMER,<sup>2</sup> GÜNTHER REDHAMMER,<sup>3,†</sup> AND GEORGE H. MYER<sup>2</sup>

<sup>1</sup>University of Marburg, Scientific Center for Materials Research and Institute for Mineralogy, 35032 Marburg, Germany

<sup>2</sup>Temple University, Department of Geology, Philadelphia, Pennsylvania 19122, U.S.A.

<sup>3</sup>University of Salzburg, Institute for Mineralogy, 8020 Salzburg, Austria

### ABSTRACT

ZrO<sub>2</sub>-EMF measurements were carried out on natural biotite samples between about 400 and 1100 °C in a closed system in a pure argon atmosphere (99.9999%). The EMF patterns are complex and cannot be compared to classical equilibrium  $1/T$ -log  $f_{\text{O}_2}$  data. Instead, the electrochemical method, when applied to hydrous phases, is a non-equilibrium, dynamic technique, comparable to differential thermal analyses. The data are interpreted from the perspective of atomic processes that control EMF readings and in light of mica-breakdown reactions known from the literature. These breakdown reactions occur at mainly three temperatures marking the onset of dehydroxylation, of oxidation, and of breakdown to oxides. The new application of ZrO<sub>2</sub>-EMF measurements proposed herein demonstrates the advantage of dynamic tracking of mica breakdown reactions; so that in a single experiment, all breakdown reactions may be studied sequentially for a specific mineral sample.

### INTRODUCTION

Any experimental study of hydrous minerals should consider their stability and composition in terms of  $P_{\text{tot}}$ ,  $P_{\text{H}_2\text{O}}$ , and, for Fe-bearing minerals,  $f_{\text{O}_2}$ . In addition, the potential breakdown of these hydrous minerals may begin at temperatures that, in the case of micas, are as low as 500 °C. The redox stability of igneous and metamorphic rocks containing micas and amphiboles involves conditions generally between the magnetite-hematite (MH) and wüstite-magnetite (WM) buffers (for a recent review see Cygan et al. 1996). To assess the relation between crystal chemistry and mica stability, heating experiments were performed historically in air or in vacuum, and synthetic mica, produced under  $f_{\text{O}_2}$ -controlled environments, was studied by Mössbauer spectroscopy (e.g., Redhammer et al. 1993). In our desire to explore the redox conditions during the genesis of natural hydrous minerals and their host rocks, we decided to investigate the suitability of the ZrO<sub>2</sub>-EMF technique. Since the pioneering work by Sato (1965, 1971) on electrochemical measurements to assess geologic oxygen fugacities, this technique has been used to investigate redox conditions of specific geologic environments (e.g., Sato 1972; Friel and Ulmer 1974; Ulmer et al. 1976; Sato and Valenza 1980; Arculus and Delano 1980, 1981; Elliott et al. 1982; Ulmer 1984; Ulmer et al. 1987; Kozul et al. 1988; Virgo et al. 1988). Zirconia elec-

trodes also have been used to obtain revised values of standard redox buffers (e.g., O'Neill and Pownceby 1993) and to monitor furnace gas  $f_{\text{O}_2}$  (e.g., Huebner 1987). In addition, the zirconia-based EMF technique is widely used as an oxygen-sensing device in industry (Claussen et al. 1984), in combustion control (Badwal et al. 1984), in automotive exhaust emission control (Muse and Soejima 1983), and in fuel cells (Huijsmans et al. 1989).

For hydrous minerals, the intended use of the ZrO<sub>2</sub>-EMF technique confronts one with at least three immediate questions. (1) In view of the conventional use of the ZrO<sub>2</sub>-EMF technique between 700 and 1100 °C, would these ZrO<sub>2</sub> cells function at low-enough temperatures? (2) Given the dehydroxylation of micas at temperatures as low as 500 °C, how would such log  $f_{\text{O}_2}$ - $T$  data compare to classical redox equilibrium measurements on non-hydrous minerals? (3) Would it be possible to interpret such, presumably dynamic, non-equilibrium data from the breakdown of hydrous minerals in relation to established mica-reaction processes?

With regard to question 1, we recently illustrated and discussed that redox systems, such as gas mixtures, conventional oxygen buffers, and Y-doped ZrO<sub>2</sub> cells, operate at low temperatures. Specifically, low temperature ZrO<sub>2</sub>-EMF measurements on buffers were reproducible and linear in  $1/T$ -log  $f_{\text{O}_2}$  to temperatures as low as 300 °C, which confirmed the reliability of this method (Burkhard et al. 1991; Burkhard and Ulmer 1995a). These results and calibrations set the stage for carrying out an initial study on oxide and silicate mineral redox stabilities

\* E-mail: burkhard@mail.uni-marburg.de

† Present address: RWTH Aachen Institute for Crystallography, 52056 Aachen, Germany.

**TABLE 1.** List of samples, their localities and references

Sample	Mineral	Locality	Reference/Source
<b>Granite samples</b>			
Berg 11b	biotite	Bergell, Southern Alps, Switzerland/Italy	Burkhard (1993)
Berg 18a	biotite	Bergell, Southern Alps, Switzerland/Italy	Burkhard (1993)
Berg 3a	biotite	Bergell, Southern Alps, Switzerland/Italy	Burkhard (1993)
Berg 19c	biotite	Bergell, Southern Alps, Switzerland/Italy	Burkhard (1993)
<b>Samples from Alkaline provinces</b>			
Ves (E10975)	phlogopite	Vesuvius, Italy probl. 72 AD eruption	Museum of Victoria (Melbourne)
Pa. 1 (E10975)	phlogopite	Palabora Carbonatite, Forskor Transvaal, South Africa	Museum of Victoria (Melbourne)
Pa. 2 (E8060)	phlogopite	Loolekop Pipe, N Transvaal, South Africa	Museum of Victoria (Melbourne) Museum of Victoria (Melbourne)
Uganda 1 (C5927)	phlogopite	Lake Kikorongo ejecta, Uganda	A. Cundari, Naples
Uganda 2 (C5691)	phlogopite	Micropyroxenite-Xenolith believed to represent metasomatized Upper mantle	A. Cundari, Naples

at these low temperatures (Burkhard and Ulmer unpublished data), including a technique-pilot study on micas (Burkhard and Ulmer 1995b). We herein report the results of our general investigation of Fe-bearing micas, purposely chosen from a wide range of geologic settings, such as granites, carbonatites, and mantle peridotites.

The  $1/T$ -log  $f_{O_2}$  patterns for these micas cannot be compared to the patterns of known equilibrium oxygen fugacity studies of non-hydrous minerals. Instead, these patterns are shown to be able to track the progress of dehydroxylation and oxidation reactions. The technique is comparable to the dynamic tracking of reactions during differential thermal analyses (DTA). In the light of literature data on mica redox and breakdown reactions, as obtained from many different techniques, we show that there is a good correlation between those reported reaction temperatures and our data. ZrO<sub>2</sub>-EMF measurements on mica can therefore, in a single experiment, provide data on reaction characteristics that heretofore have required a series of separate experiments such as thermal gravimetric analyses (TGA), DTA, infrared analyses (IR), X-ray diffraction (XRD), and Mössbauer spectroscopy.

## METHOD AND PROCEDURE

### Sample selection and separation

Biotite separates were prepared from fresh rock samples. They had no or only minor alteration such as chloritization, and had as few inclusions as possible. Sample location and further descriptions are given in Table 1.

Because EMF measurements are very sensitive to any reducing agent such as organics, metals, or carbides introduced during sample preparation of which even traces would dominate the signal, special care was taken during the mineral separation to avoid any contact with such agents. Rock samples were diamond-sawed into cubes, wrapped in paper and then crushed gently with a hammer. The fragments were sieved with a 1 cm × 500 μm × 250 μm sieve arrangement, washed in distilled water, and dried at 60 °C. Flakes were separated from mica fractions between 500 μm and 1 cm mica "books," and more granular mica was separated from the fractions between 250

and 500 μm. Final hand-picking under a binocular microscope was carried out to obtain a purity of better than 99%.

### Method

The electrochemical method detects a voltage between two sides of a specific-ion-membrane that separates phases or environments of different activities, or fluids of different fugacity (partial pressure). The use of a standard of known activity or fugacity on one side of the membrane allows one to convert the developed voltage (EMF) to the activity or fugacity of the unknown at the other side through the Nernst equation. The membrane commonly used to sense oxygen fugacity ( $f_{O_2}$ ) is ZrO<sub>2</sub>, doped with either Y<sub>2</sub>O<sub>3</sub> or CaO to stabilize the ZrO<sub>2</sub> cubic polymorph and to improve mechanical stability over a wide temperature range. Furthermore, the dopant creates oxygen vacancies that are necessary for the development of the EMF.

Here, EMF measurements were taken with ZrO<sub>2</sub> cells doped with 8 wt% Y<sub>2</sub>O<sub>3</sub>. The cells were arranged in the same double-cell setup described in detail in Burkhard and Ulmer (1995a). In brief, the double-cell arrangement uses a well-defined CO<sub>2</sub>-H<sub>2</sub> gas mixture called the furnace gas (FCE), which "bridges" the two cells. The mixing ratio of CO<sub>2</sub>-H<sub>2</sub> FCE gas is 100/1 (i.e., log mixing ratio +2). While the bottom cell reads the EMF for air against FCE, the top cell, containing the mica sample (typically about 20 mg) in a Ag<sub>60</sub>Pd<sub>40</sub> bucket, reads the EMF of the sample against the FCE. Subsequent to sample loading, this top ZrO<sub>2</sub> cell was vacuum-flushed with ultra-pure Ar (99.9999%) through five cycles and finally filled with this Ar at a pressure of 1.33 × 10<sup>5</sup> Pa. The Ar-filled free space equals about 1 cm<sup>3</sup>. According to PVT-relationships for Ar as an ideal gas, pressure increases to 6.3 × 10<sup>5</sup> Pa at the peak temperature of 1100 °C of the experiments, which could also be confirmed experimentally. EMF data, taken with a high impedance Keithley 619 voltmeter (10<sup>14</sup> Ohm), were converted to log  $f_{O_2}$  values using the Nernst equation,  $\log f_{O_2} = -\Delta E/0.0496 T$  ( $T$  in Kelvin), taking into account correction procedures described in Burkhard

and Ulmer (1995a). Ar blank tests showed that the  $f_{\text{O}_2}$  is temperature independent, commensurate with the 99.9999% purity of Ar, and that therefore neither air nor furnace gas leaked into the top cell.

Depending on the temperature at which we first observed an electrical contact upon heating, the EMF data acquisition started between 400 and 500 °C and was carried out up to about 1100 °C in steps of 10 to 40 degrees. All EMF data were taken after temperature was stabilized ( $\pm 2$  °C), which was generally the case within minutes after reaching the set temperature. Depending on the specific stage of the experiment, EMF readings were either "steady-state" or "non-steady-state." We define steady-state values as being stable within minutes, and steady within  $\pm 1$  mV over 20 min (shown in solid symbols hereafter), yet this does not imply that these were necessarily equilibrium data (see discussion). We define the non-steady-state readings as those that occurred at some characteristic temperatures,  $T_1$  and  $T_2$ , at which the EMF did not stabilize. Instead, the voltage increased continuously over a period of 7 h or longer (shown as open symbols to emphasize their special dynamic nature). After these long holds at the temperature of such non-steady-state behavior, subsequent cooling and re-heating was found to follow a steady-state  $f_{\text{O}_2}$ - $T$  path. The usual time for a biotite run was around 14 to 18 h. In at least one case (Berg3a), enough sample was available for duplicate runs, which proved reproducibility of the  $f_{\text{O}_2}$ - $T$  path and characteristic temperatures within experimental error.

#### Chemical analyses, X-ray diffraction, and Mössbauer spectroscopy

To characterize the mica and to detect possible changes of the redox state caused by the EMF experiment, we analyzed the original and the heat-treated samples (where sample preparation was possible), using a Cameca SX-50 electron microprobe operating at 15 kV and 25 nA. Natural standards were used for Si, Ca (wollastonite), Mg (periclase), Fe (hematite), Ti (rutile), Na (jadeite), Ba (benitoite), K (in a pyrochlore), Cl (NaCl), and P (apatite); synthetic standards were used for Al ( $\text{Al}_2\text{O}_3$ ), F ( $\text{NaAlF}_4$ ), and for Cr, Mn, and Zn (pure elements). Small run products of 20 mg did not permit further meaningful routine investigations. However, in one case (Uganda 2), despite unavoidable orientation-related textural effects, an investigation with XRD could be performed before and after the EMF measurement. These XRD data were obtained with a Rigaku DMAXB computer-controlled horizontal goniometer, equipped with a standard focus Cu tube (45 kV and 30 mA). A curved-crystal graphite monochromator filtered the diffracted beam. The continuous scan mode for the pattern was set at a range of 2–90° 2 $\theta$  with a sampling interval of (0.05°) and a scan rate of 2°/min. External calibration of the goniometer is based on silicon powder (NBS 640b), and intensity measurements are based on internal calibration with cerium oxide (NBS 674a). The mica samples were prepared without further grinding. Slurries of mica were evaporated on

quartz plates to produce minimal background patterns. The preparations were re-slurried and multi-scanned to produce an averaged result for peak position and intensity.

On three samples, Berg3a, Berg11, and Pa2, we carried out  $^{57}\text{Fe}$  Mössbauer spectroscopy (300 K) to compare the Fe-valence state in the micas, both before and after the EMF measurements. Spectra were collected on a conventional spectrometer (Fa. Halder Electronics, Germany) running in constant acceleration mode with triangular velocity shape, 1024 channel MCA, and horizontal arrangement of the  $^{57}\text{Co}/\text{Rh}$  source, absorber, and detector. To avoid texture effects arising from oriented mica flakes, the absorber was placed at 54° (magic angle) to the incident  $\gamma$ -rays (Ericsson and Wäppling 1976). Any crushing necessary in the course of the absorber preparation (thickness 2.5 mg Fe/cm<sup>2</sup>) was done under acetone for no more than 2–3 min to avoid oxidation. For absorber preparation, the mica powder was carefully mixed and homogenized with powdered sugar and filled into copper-rings with an inner diameter of 10 mm and a thickness of 2 mm. Spectra were usually run until an off-resonant count of at least  $2 \times 10^6$  counts per channel was reached. All spectra were calibrated to an  $\alpha$ -Fe foil and were analyzed by least-squares refinement assuming Lorentzian line shapes of symmetric doublets with the program MOESALZ (Lottermoser et al. 1992).

Spectra were refined using up to 5 doublets corresponding to octahedral Fe<sup>2+</sup> (M1 and M2) as well as octahedral (M1 and M2) and tetrahedral Fe<sup>3+</sup>. According to previous studies, the Fe<sup>2+</sup> doublet with the larger splitting was assigned to an M2-like configuration, the inner one corresponds to an M1-like configuration. For Fe<sup>3+</sup>, the assignment was done vice-versa (Annersten et al. 1974; Dyar and Burns 1986; Dyar 1990; Redhammer et al. 1993, 1995). It should be emphasized that quantitative M2/M1 occupancy ratios for Fe<sup>3+</sup> or Fe<sup>2+</sup> cannot be deduced from Mössbauer spectra alone. In contrast, Fe<sup>2+</sup>/Fe<sup>3+</sup> ratios as well as  $\Sigma(\text{VI Fe}^{2+} + \text{VI Fe}^{3+} + \text{IV Fe}^{3+})$  can be extracted with high accuracy. However, the assignment of Fe<sup>2+</sup> doublets to specific crystallographic sites in micas is a point of current discussion (Rancourt et al. 1994a, 1994b; Rancourt 1994a, 1994b; Redhammer 1996).

## RESULTS

In contrast to an essentially linear relationship between  $\log f_{\text{O}_2}$  and  $1/T$  for conventional equilibrium studies of anhydrous minerals, the data on the micas presented here-in follow a complex pattern. Based on the shape of the  $\log f_{\text{O}_2}$  vs.  $1/T$  plots, we distinguished three types of mica patterns: Type a shown in Figure 1, and Types b and c shown in Figure 2. General characteristics are illustrated schematically in Figure 3. Types a and b are in principle similar, except that the Type b pattern is shifted by several log units of  $f_{\text{O}_2}$  to more oxidized conditions. Microprobe analyses are listed in Table 2, and Mössbauer data in Table 3.

## Type (a)

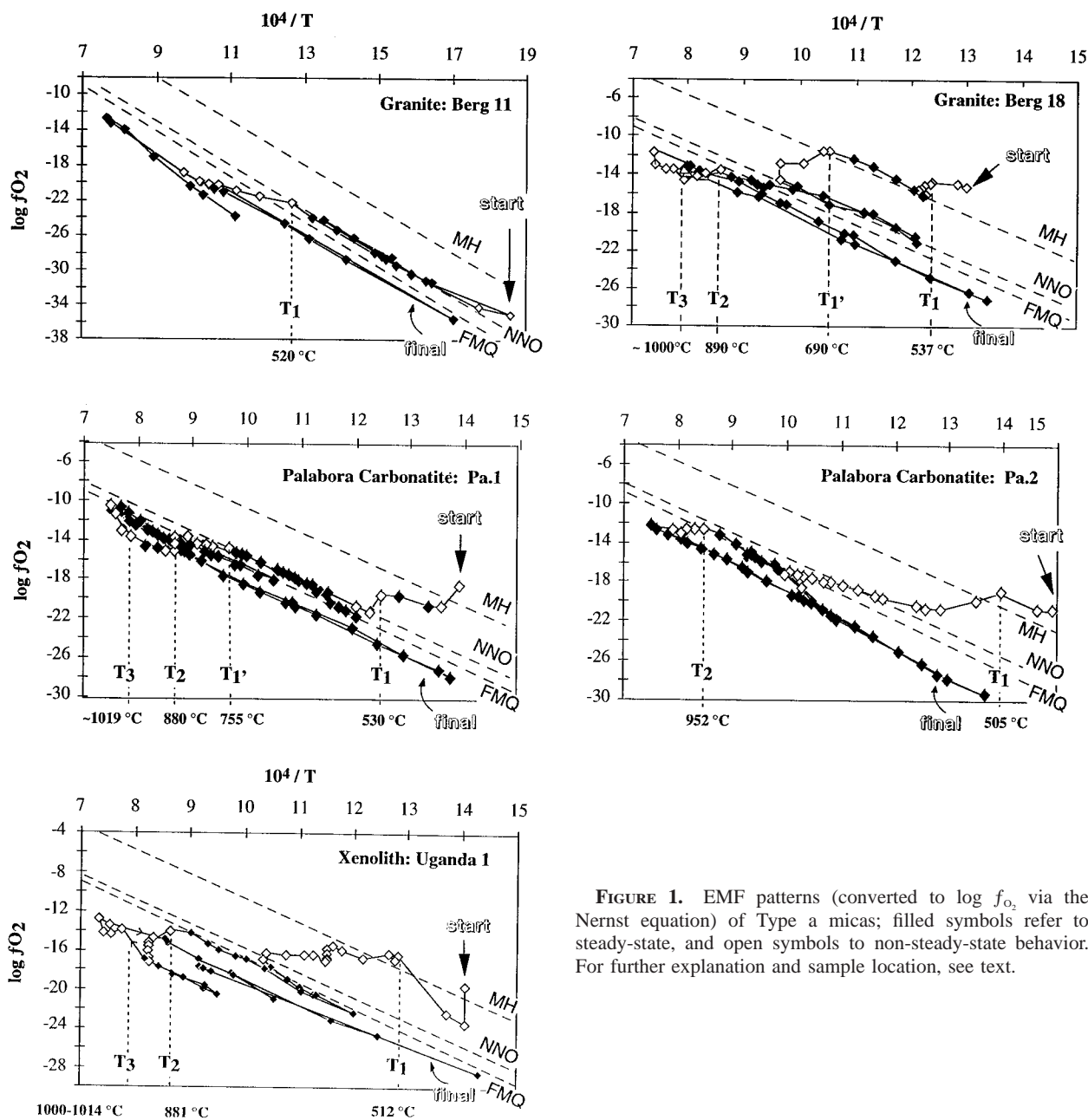


FIGURE 1. EMF patterns (converted to  $\log f_{O_2}$  via the Nernst equation) of Type a micas; filled symbols refer to steady-state, and open symbols to non-steady-state behavior. For further explanation and sample location, see text.

### Overview of Type a and Type b

On the initial heating path,  $f_{O_2}$  values were, as a rule, oxidized and on the cooling path,  $f_{O_2}$  values were more negative. Specifically, when cooling from 1100 °C, values dropped by 0.5 to 4 log units below the FMQ buffer for Type a, and approached the FMQ or NNO buffers for Type b. All closed data points in Figures 1 and 2 show steady-state data. Here, similar  $T$ - $\log f_{O_2}$  values were

measured, after going down and up temperature. At certain temperatures,  $T_1$ ,  $T_2$ , and  $T_3$  (Figs. 1–3), the  $T$ - $f_{O_2}$  phenomena were non-steady-state and the EMF changed significantly with time (open data points in the figures). The onset of such non-steady-state behavior was dependent on the heating rate (not slower than 10 °C steps per quarter hour with temperature holds at each step). The analogy of this non-steady state behavior to DTA or DSC

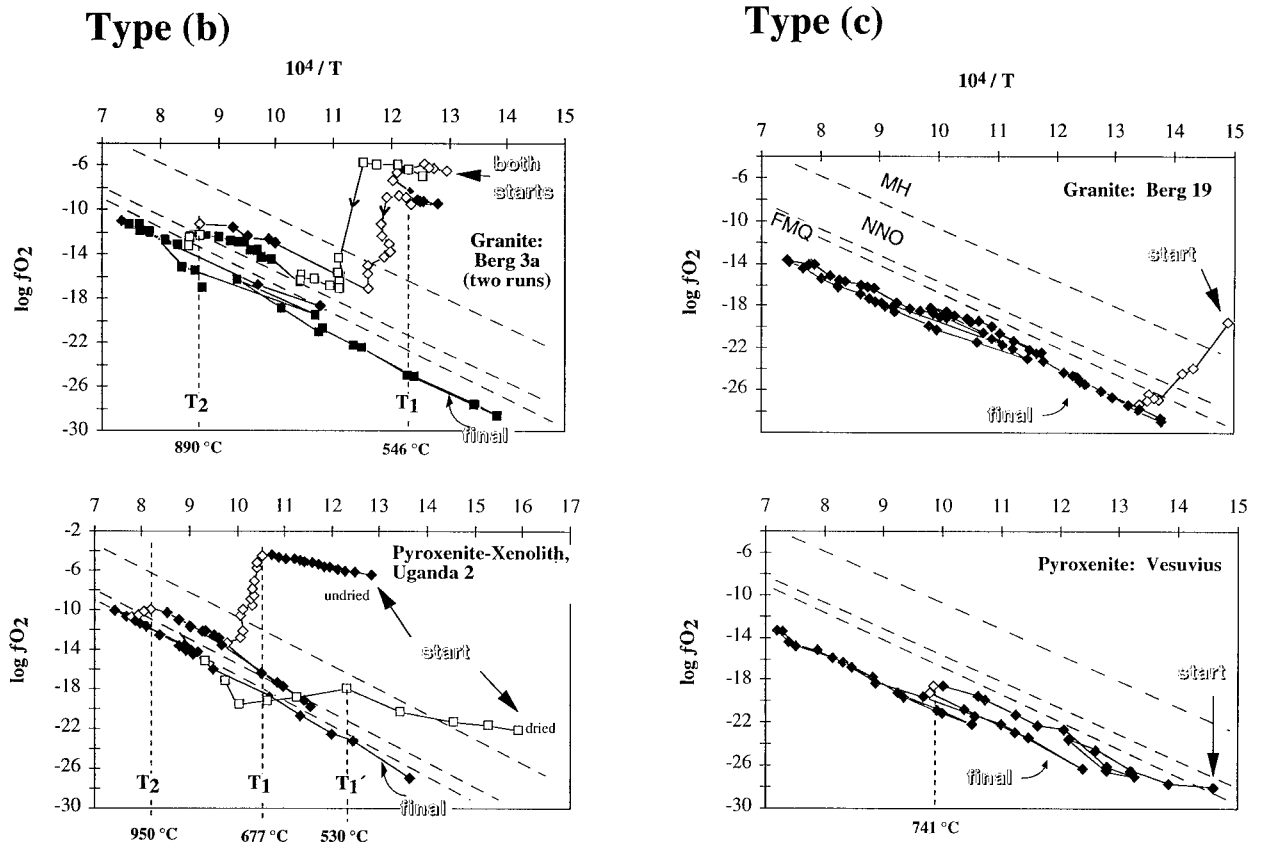


FIGURE 2. EMF pattern of Type b and Type c micas (filled symbols: steady-state, open symbols: non-steady-state behavior). Type b is similar to Type a micas, but the patterns are shifted to more oxidized values. Type c contains carbon, which dominates any other EMF signal. For further explanation and details on samples, see text.

experiments, where heating rates often outrun the reaction rate but nevertheless reveal the reaction process/progress, suggests that the onset of the non-steady-state behavior at  $T_1$ ,  $T_2$ , and  $T_3$  marks the onset of reactions.

#### Type a

Type a represents the “normal case” (Burkhard and Ulmer 1995b); five examples are shown in Figure 1. Starting EMF values calculate to  $f_{O_2}$  values in the vicinity of the MH buffer<sup>1</sup>. The patterns are characterized by a later marked increase in EMF (decrease in  $f_{O_2}$ , relative to the buffers) at two characteristic temperatures,  $T_1$  and  $T_2$ , between 505 and 540 °C and between 880 and 950 °C, respectively. In some cases, a third temperature,  $T_3$ , around 1000 °C can be distinguished where the EMF decreases ( $f_{O_2}$  increases, relative to buffers) upon heating.

<sup>1</sup> Data were collected as a voltage, the EMF values. For convenience and the sake of comparison, we have plotted  $\log f_{O_2}$ , obtained by converting the EMF signal via the Nernst equation. However, since  $f_{O_2}$  implies equilibrium conditions, which we do not claim to have at every stage of our dynamic measurement, we refer to the actual EMF signal when discussing the dynamic of the pattern.

#### Type b

Two examples of Type b are presented in Figure 2. These micas show an overall pattern similar to Type a, except for a shift to much more oxidized values and, specifically, a much more oxidized start. To investigate the reason for these oxidized values, we repeated an EMF measurement on one of these micas, Uganda 2, after drying overnight at 115 °C. Figure 2 compares the pattern of the dried sample to that of the first undried sample, plotted in one graph. The starting  $\log f_{O_2}$  values of the dried sample are comparable to those of Type a and are more negative by 12 log units than those of the undried sample. Furthermore, with pre-drying, the first major slope change, marking  $T_1$ , occurs at a lower temperature than without pre-drying ( $T_1$ ). This suggests that drying removed surface-adsorbed volatiles and that they were responsible for the highly oxidized starting values of the first experiment and delayed the reaction at  $T_1$ . In addition, we carried out effluent gas analyses of  $CO_2$  and  $H_2O$  on Uganda 2, and compared the results to a mica that showed a different EMF pattern, Berg 19, a Type c mica (see below). After heat treatment in an Ar atmosphere at 780 °C for 2.5 h, sample Uganda 2 showed 87 ppm of

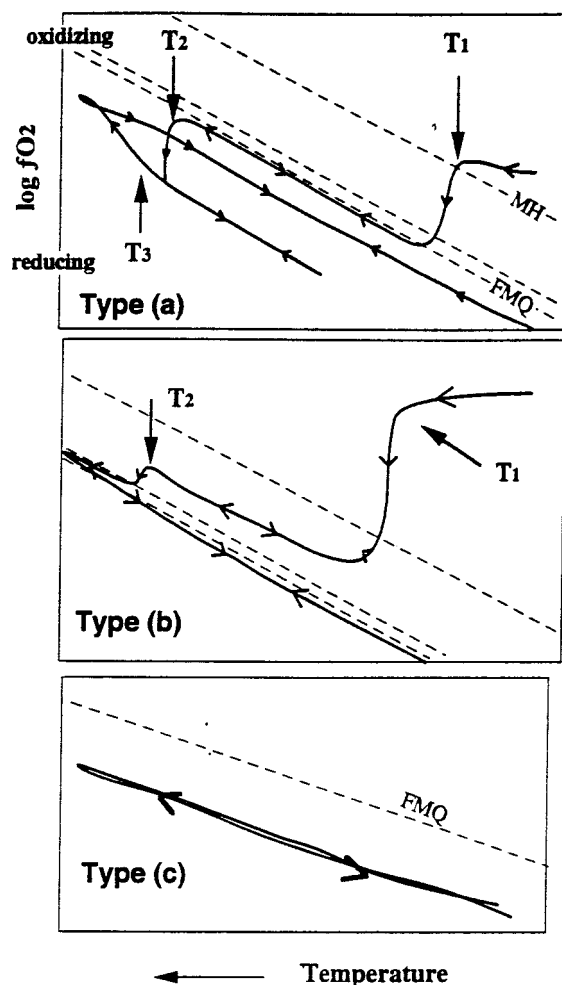


FIGURE 3. A schematic sketch of the three mica types a, b, and c with their characteristic features, i.e. reaction temperatures and redox state at the beginning, during, and after the EMF experiment. Arrows in two directions mark the steady-state behavior and arrows in one direction mark the non-steady-state behavior.

CO<sub>2</sub> and 25 ppm of H<sub>2</sub>O. Sample Berg 19, heated to 1100 °C for 1 h, showed only 15 ppm H<sub>2</sub>O. CO<sub>2</sub> and H<sub>2</sub>O released from Uganda 2 should include surface adsorbed water, in addition to possible structurally bonded volatiles or even inclusions, although we did not observe any inclusions optically. The mass balance of these gases and their own  $f_{O_2}$ - $T$  values, when added to the 1 cm<sup>3</sup> of 99.9999 pure inert Ar in the cell, is consistent with the highly oxidized starting values.

#### Type c

Two examples of Type c have log  $f_{O_2}$  values below FMQ, during the initial heating as well during the cooling (Fig. 2). In both cases (Berg 19 and Vesuvius), we found carbon to have precipitated on the colder portions of the Vycor filler rod. This type of carbon precipitation occurs when CO<sub>2</sub> (and hence also CO) is present within the ZrO<sub>2</sub>

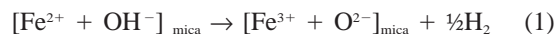
cell. Carbon precipitation in such situations has been discussed in theory by Deines et al. (1974) and in the ZrO<sub>2</sub> cell by Virgo et al. (1988). EMF experiments on mineral phases associated with these micas in the rock (olivine and magnetite), not shown here, in each case resulted in carbon precipitation on the Vycor filler rod. Therefore, and because all mica samples were prepared in the same way, we do not feel that the reducing agent is a contaminant. Effluent gas analyses of Berg 19, as mentioned above, showed only a small amount of water (15 ppm) and no CO<sub>2</sub> or CO (<1 ppm). In light of the influence of volatiles on the EMF reading, as observed for Type b mica (see above), this carbon would reduce H<sub>2</sub>O to provide the overall reducing atmosphere measured in the cell.

#### Redox state

A comparison of the chemical composition of mica samples prior to and after the run, (based on an average of 3 to 8 microprobe analyses each) shows that the formula proportions of cations agree within a systematic error on the order of 0.1 wt% (Table 2). Mössbauer data on micas before and after the EMF experiment, however, reveal significant changes of the redox state; all micas have undergone a pronounced oxidation, and Fe<sup>3+</sup> has increased by factors of 2.8 (Berg 11b), 3.3 (Berg 3a), and 10.8 (Pa2), as shown by data in Figures 4a to 4f and Table 3. The total Fe<sup>2+</sup> and Fe<sup>3+</sup> of these micas, before and after the experiments (Table 3), are reliable to ±2%. However, the assigned distribution between the M1 and M2 sites should be considered tentative and with caution.

#### DISCUSSION

The non-steady-state behavior at the temperatures  $T_1$ ,  $T_2$ , and  $T_3$  for mica Types a and b suggests that specific mineral breakdown reactions have taken place. Mica breakdown, in relation to oxidation upon heating, was first described for the pure iron end-member biotite (annite) as the "oxyannite substitution" (Rinne 1924). Upon heating, biotite is converted to oxybiotite by a coupled mechanism, whereby Fe<sup>2+</sup> and an hydroxyl react by electron transfer to Fe<sup>3+</sup> and hydrogen. The general oxidation reaction is usually written as:



(e.g., Rimsaite 1970; Vedder and Wilkinson 1969; Farmer et al. 1971; Veith and Jackson 1974; Ross and Rich 1974; Tripathi et al. 1978; Hogg and Meads 1975; Bagin et al. 1980; Sanz et al. 1983).

To understand the diversity of EMF patterns and how electrochemical measurements track dynamically the breakdown reactions of micas, we shall first consider the nature of EMF measurements, then review the literature on mica stability with respect to dehydration and oxidation reactions as reported in previous studies, based on IR spectroscopy, TGA, and Mössbauer spectroscopy. We shall then relate these concepts to our EMF data and to the final redox state of the samples.

TABLE 2. Electron microprobe analyses of the mica (average of 3 to 5 analyses)

	Type a					Type b					Type c		
	Berg 11b	Berg 11 b/u	Berg 18	Uganda1/u	Pa 1u	Pa2	Pa 2/u	Berg 3a	Berg3a/heat	Berg3a/u	Uganda2	Berg 19c/u	Ves/crush
SiO <sub>2</sub>	36.62	37.26	36.50	37.14	41.37	42.17	42.09	36.47	36.39	36.77	37.91	37.32	38.57
TiO <sub>2</sub>	2.97	2.77	2.11	5.47	0.57	0.84	0.82	2.88	2.83	2.73	6.25	2.89	2.54
Al <sub>2</sub> O <sub>3</sub>	13.98	14.91	14.88	12.53	7.63	9.70	9.71	15.39	15.57	15.34	13.66	14.65	14.70
Cr <sub>2</sub> O <sub>3</sub>	0.02	0.04	—	0.06	0.02	0.02	0.02	0.03	0.02	0.01	—	0.02	0.05
MgO	10.92	11.18	11.29	16.30	24.06	24.72	24.65	10.14	10.40	10.38	18.86	11.48	21.49
CaO	0.00	0.00	—	0.00	0.00	0.00	0.00	0.00	0.00	0.00	0.07	0.01	0.00
MnO	0.39	0.37	0.32	0.10	0.05	0.04	0.06	0.53	0.49	0.52	0.04	0.37	0.04
FeO	19.49	19.42	20.90	13.21	10.57	6.94	7.00	19.00	18.52	19.88	8.33	19.05	6.90
ZnO	0.07	0.02	0.13	0.03	0.03	0.01	0.01	0.06	0.06	0.05	0.03	0.05	0.04
BaO	0.03	0.04	0.04	0.16	0.07	0.07	0.07	0.06	0.03	0.05	—	0.03	0.46
Na <sub>2</sub> O	0.07	0.08	0.07	0.34	0.06	0.01	0.01	0.08	0.09	0.09	—	0.11	0.27
K <sub>2</sub> O	8.92	9.24	8.99	9.00	10.05	9.72	9.79	8.81	9.06	9.23	9.98	9.32	9.07
P <sub>2</sub> O <sub>5</sub>	0.00	0.00	—	0.01	0.00	0.00	0.01	0.01	0.00	0.00	—	0.00	0.01
F	0.44	0.41	0.31	0.22	0.86	0.53	0.53	0.65	0.64	0.63	0.01	0.41	0.55
Cl	0.02	0.02	0.03	0.01	0.04	0.00	0.00	0.02	0.02	0.02	0.29	0.02	0.03
total	93.94	95.77	95.57	94.59	95.39	94.79	94.76	94.13	94.13	95.71	95.43	95.74	94.71
O = F, Cl	0.19	0.18	0.14	0.10	0.37	0.22	0.22	0.28	0.27	0.27	0.07	0.18	0.24
Formula proportions based on 24 (O, OH, F, Cl)													
Si	5.706	5.680	5.709	5.583	6.133	6.114	6.110	5.660	5.641	5.642	5.525	5.687	5.615
Al (IV)	2.294	2.320	2.291	2.220	1.334	1.658	1.661	2.340	2.359	2.358	2.347	2.313	2.385
Ti (IV)	0	0	0	0.197	0.063	0.092	0.090	0	0	0	0.128	0	0
Σ tetr.	8.000	8.000	8.000	8.000	7.530	7.865	7.861	8.000	8.000	8.000	8.000	8.000	8.000
Al (VI)	0.274	0.358	0.478	0.000	0	0	0	0.475	0.485	0.417	0	0.317	0.137
Ti (VI)	0.348	0.318	0.252	0.421	0	0	0	0.337	0.330	0.314	0.557	0.332	0.278
Cr	0.002	0.004	—	0.008	0.003	0.002	0.002	0.004	0.002	0.002	0.000	0.002	0.006
Mg	2.538	2.540	2.668	3.653	5.318	5.343	5.335	2.345	2.404	2.375	4.098	2.608	4.663
Ca	0	0	—	0	0	0	0	0	0	0	0.011	0.002	0
Mn	0.052	0.048	0.044	0.013	0.006	0.005	0.007	0.069	0.064	0.068	0.005	0.047	0.005
Fe	2.540	2.476	2.473	1.661	1.310	0.842	0.850	2.466	2.401	2.551	1.016	2.427	0.840
Zn	0.008	0.003	0.015	0.003	0.003	0.002	0.001	0.007	0.007	0.005	0.003	0.005	0.004
Ba	0.002	0.002	0.002	0.009	0.004	0.004	0.004	0.004	0.002	0.003	0.000	0.002	0.026
Na	0.020	0.023	0.023	0.099	0.018	0.003	0.004	0.024	0.027	0.028	0.000	0.032	0.077
K	1.773	1.798	1.890	1.726	1.901	1.798	1.812	1.745	1.791	1.806	1.856	1.812	1.684
P	0.000	0.001	—	0.002	0.000	0.000	0.001	0.001	0.001	0.001	0.000	0.000	0.001
F	0.216	0.196	0.213	0.106	0.405	0.243	0.244	0.317	0.314	0.305	0.003	0.198	0.254
Cl	0.008	0.007	0.010	0.003	0.012	0.001	0.001	0.008	0.008	0.009	0.102	0.008	0.010
OH	3.776	3.797	3.717	3.891	3.583	3.756	3.756	3.675	3.678	3.686	3.894	3.793	3.736

Note: u = used in an EMF experiment; heat = heat-treatment in a non-EMF experiment; crush = big flakes had to be ground slightly. (OH) = 4 - (F + CL).

### The EMF signal

The basic concept of oxygen sensors, such as doped-ZrO<sub>2</sub>, is the detection of a charge potential caused by different concentrations of oxygen on two sides of such a membrane. Essential for the conversion of a concentration to a detectable charge potential is the use of a catalyst, which is typically Pt, in contact with the ZrO<sub>2</sub> (for a review, see Miyamoto and Mikouchi 1996). In our setup, Ag<sub>60</sub>Pd<sub>40</sub> was used because it is less apt to alloy with the transition elements in the sample. On the surfaces of Ag<sub>60</sub>Pd<sub>40</sub>, O<sup>2-</sup> from the mica is chemisorbed and thus provides the charge potential. It is this process of chemisorption that triggers the EMF measurement in what would otherwise be neutral molecular gas species. Not only O<sup>2-</sup> but also any other substance may equally be chemisorbed on the noble metal surfaces and thus influence the EMF signal (e.g., Burkhard and Ulmer 1995a, Fig. 6). Specifically, in the course of our EMF experiment, mica breakdown may release not only O<sub>2</sub>, but also hydroxyls, H<sub>2</sub>O and H<sub>2</sub>. In some cases, even CO, CO<sub>2</sub>, or halogens may be released, as discussed below. Since each

hydroxyl, if chemisorbed as OH<sup>-</sup>, contributes only one negative charge, it gives rise to a smaller EMF signal than oxygen, chemisorbed as O<sup>2-</sup>. H<sub>2</sub> should increase the EMF signal to a more reducing log *f*<sub>O<sub>2</sub></sub> value because it either attracts oxygen already chemisorbed, or is itself chemisorbed, dissociates, and thus provides two positive charges. Any H<sub>2</sub>O, if chemisorbed, dissociates into OH<sup>-</sup> and H<sup>+</sup>, which in total is neutral. In principle, H<sub>2</sub>O should therefore not influence the EMF signal unless the dissociation products back-react into the mineral. Alternatively, the H<sub>2</sub>O may impart an oxidizing effect if hydrogen escapes. However, the data do not support any mechanical leakage of H<sub>2</sub>, nor is H<sub>2</sub> or H<sup>+</sup> expected to migrate along vacancies of positive holes in the ZrO<sub>2</sub> cell. Finally, if CO<sub>2</sub> is liberated from the mica surface, it is chemisorbed on the PdAg surface, by bending the straight 180° angle of O = C = O, followed by dissociation to CO and O<sup>2-</sup> (Bartos et al. 1986). This oxygen may either directly decrease the EMF or it may react with H<sub>2</sub>, present in the system, forming OH<sup>-</sup>. In either case, CO<sub>2</sub> will decrease the EMF (increase *f*<sub>O<sub>2</sub></sub>).

**TABLE 3.** Mössbauer spectroscopic data of three mica samples, each before and after (“u”) the EMF experiment

	Total Fe <sup>2+</sup> in M1, M2	Total Fe <sup>3+</sup> in M1, M2, tetr.	Change in Fe <sup>3+</sup> /Fe <sup>2+</sup>	Fe <sup>2+</sup> M1				Fe <sup>2+</sup> M2			
				IS	ΔEq	Γ	A	IS	ΔEq	Γ	A
Pa.2*	74	26	0.22	1.12	2.36	0.36	35	1.10	2.68	0.27	39
Pa.2 u.	39	61		1.11	2.34	0.41	17	1.11	2.65	0.31	22
Berg 11	88	12	0.26	1.12	2.23	0.45	51	1.12	2.66	0.28	37
Berg 11 u.	66	34		1.10	2.16	0.51	45	1.11	2.63	0.37	21
Berg 3a	82	18	0.14	1.07	2.18	0.40	34	1.11	2.59	0.31	48
Berg 3a u.	41	59		1.11	2.16	0.54	34	1.12	2.90	0.26	7
Average				1.09	2.26			1.12	2.57		
Dyar (1990)				(0.02)	(0.13)			(0.02)	(0.12)		

Notes: IS = isomer shift [mm/s]; ΔEq = quadrupole splitting [mm/s]; Γ = full width at half maximum [mm/s]; IS, ΔEq, Γ = ±0.02 mm/s; A = ±2%. A = relative intensity (area) [%].

\* Values given for Fe<sup>3+</sup> are intermediate between M1 and M2.

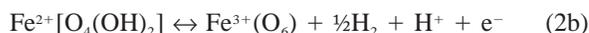
### Literature review: Biotite stability during heating

The stability of biotite has found much interest in Earth sciences and ceramic industry. While phase equilibria were considered by Yoder and Eugster (1954), Eugster and Wones (1962), and Wones and Eugster (1965), another focus has been biotite stability in relation to dehydroxylation and oxidation. The mechanism of dehydroxylation has been investigated by TGA and by IR spectroscopy, whereas the oxidation state has been evaluated mainly by Mössbauer spectroscopy. From this background, the “oxyannite” component (Eq. 1) has been established. More specifically, one finds that in vacuum H<sub>2</sub> is released, whereas in air environmental oxygen becomes involved leading to the release of H<sub>2</sub>O (Farmer et al. 1971; Hogg and Meads 1975). The research on dehydroxylation and oxidation, carried out mainly in air, but in some cases also in vacuum, suggests the following three-step reaction (e.g., Vedder and Wilkins 1969; Tripathi et al. 1978; Rancourt et al. 1993). The first step is the liberation of the least tightly bonded OH<sup>-</sup> associated with empty octahedral sites, between 300 to 600 °C, in vacuum (Tripathi et al. 1978; Sanz et al. 1983). With increasing temperatures, dehydroxylation continues together with oxidation, starting below 400 °C in an oxidizing environment, but not below 800 °C in an oxygen-poor environment (Hogg and Meads 1975). For Fe-poor biotite, oxidation starts as low as 280 °C (Tripathi et al. 1978). The second step involves oxidation, occurring with increasing temperature in three continuous reactions that expel one electron and hydrogen (Rimsaite 1970; Hogg and Meads 1975; Tripathi et al. 1978):

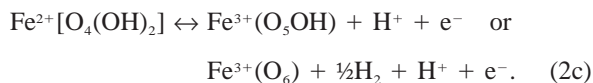
Fe<sup>2+</sup> in cis-M2 isolated octahedral sites:



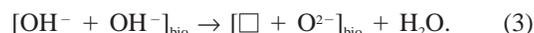
Fe<sup>2+</sup> in adjacent cis-M2 octahedral sites:



Fe<sup>2+</sup> in cis-M2 and trans-M1 sites:



Third, investigations in air at higher temperatures suggest that above 1000 °C dehydroxylation affects those OH<sup>-</sup> groups that are linked to ions other than Fe, such as Mg<sup>2+</sup> (Tripathi et al. 1978; Hogg and Meads 1975; Vedder and Wilkins 1969), leaving a vacancy □, by the reaction:



According to Hogg and Meads (1975), this reaction is possibly equivalent to, or it initiates, the final structural mica breakdown to oxides, including Fe<sub>2</sub>O<sub>3</sub> at 900–1000 °C in air.

### EMF pattern of Type a and Type b mica

At  $T < T_1$ . Any heating process up to 220 °C releases surface-adsorbed or loosely bonded molecular water (e.g., Van der Waals bonding) and, at temperatures around 300 °C, dehydroxylation starts (Knauth and Epstein 1982; Sanz et al. 1983) according to step 1. Starting conditions for our experiments with samples in an Ar atmosphere, even up to  $6.3 \times 10^5$  Pa, should resemble vacuum conditions. As illustrated with the example of Uganda 2, high  $f_{\text{O}_2}$  values and an oxidizing environment, observed for Type a and specifically for Type b biotite, are consistent with released surface H<sub>2</sub>O and possibly also CO<sub>2</sub> (effluent gas analyses), and with dehydroxylation. One should realize that any gas released upon heating cannot disappear out of the cell by diffusion and will remain in the system during the entire experiment.

At  $T_1$  and  $T_2$ . Continued heating of Types a and b mica showed that the EMF increases ( $f_{\text{O}_2}$  becomes more negative) at a characteristic temperature  $T_1$ , between 470 and 550 °C, depending on the mica sample, and in some cases also at  $T_2$ , around 880 °C. This observation is consistent with oxidation to Fe<sup>3+</sup>, related to the concomitant expulsion of H<sub>2</sub> documented in Equations 2a–c because H<sub>2</sub> should produce a reducing signal.  $T_1$  and  $T_2$  should therefore mark the onset of biotite oxidation, the result of which is seen in the Mössbauer effect of the final products (Fig. 4a–f, and Table 3). H<sub>2</sub>, once liberated, cannot react reversibly with the mica but will be present in the atmosphere of the cell. This irreversible reaction is reflected in the non-steady-state portion of the 1/T-log  $f_{\text{O}_2}$  pattern.

TABLE 3—Extended

Fe <sup>3+</sup> M2				Fe <sup>3+</sup> M1				Fe <sup>3+</sup> tetr.			
IS	$\Delta E_q$	$\Gamma$	A	IS	$\Delta E_q$	$\Gamma$	A	IS	$\Delta E_q$	$\Gamma$	A
0.39	1.05	0.48	4	—	—	—	—	0.45	0.54	0.38	22
0.43	0.85	0.46	12	0.39	1.52	0.59	31	0.16	0.51	0.45	18
0.42	0.50	0.28	4	0.42	0.95	0.33	8	—	—	—	—
0.40	0.91	0.37	15	0.43	1.40	0.45	19	—	—	—	—
0.39	0.61	0.37	13	0.47	1.00	0.32	5	—	—	—	—
0.40	0.97	0.39	24	0.43	1.44	0.54	35	—	—	—	—
0.39	0.69	—	—	0.39	0.99	—	—	—	—	—	—
(0.02)	(0.10)	—	—	(0.03)	(0.16)	—	—	—	—	—	—

According to comparative studies (Ferrow 1987), the oxidation of Fe<sup>2+</sup> in M2 is “faster” and “easier” than the oxidation of Fe<sup>2+</sup> in M1. From activation energy considerations, we infer that lower temperatures ( $T_1$ ) would initiate the easier oxidation (Eq. 2a) and higher temperatures ( $T_2$ ) the more difficult oxidation (Eq. 2c). In some samples, a third and intermediate temperature ( $T_1'$ ) may be recognized, all with a non-steady-state increase in EMF (decrease in  $f_{O_2}$ ). It is possible, therefore, that the onset of reactions seen at  $T_1$ ,  $T_1'$  and  $T_2$  correspond to the oxidation Equations 2a, 2b, and 2c, respectively.

In addition to natural samples, we considered a synthetic hydroxy-fluorophlogopite with about 1.8 wt% H<sub>2</sub>O and <100 ppm total iron (Hatch et al. 1957). The EMF experiment, carried out after pre-drying at 110 °C, shows the Type a pattern that starts above the MH buffer. Non-steady-state behavior occurs at a higher temperature,  $T_1$  at 628 °C, and  $T_2$  at 840 °C (Fig. 5). The fact that we observe breakdown temperatures illustrates that the EMF technique indeed senses dehydroxylation and hydrogen, the release of which is related to oxidation in more Fe-rich samples. The high sensitivity is provided by the high purity of Ar used whereby one part per million of OH, hydrogen, or oxygen determines by mass balance the EMF reading. Fluorine (F<sup>-</sup>), despite its similar anion radius to O<sup>2-</sup>, is not detected by ZrO<sub>2</sub> cells (Bourcier et al. 1987)<sup>2</sup>.

Samples Pa2 and Uganda 2 show a markedly higher  $T_2$  of 950 °C. Both these samples are Mg rich and hence have less Fe<sup>2+</sup> to be oxidized. Pa2 corresponds to an Al-undersaturated ferri-phlogopite with 22% of the total Fe as Fe<sup>3+</sup> on the tetrahedral site (see Tables 2 and 3). Relative to the total amount of Fe, more Fe<sup>2+</sup> was oxidized in sample Pa2 than in samples Berg 3a and Berg 11. The increase in  $T_2$  by 60–70 degrees for Pa2, compared to the other micas, suggests that oxidation is sluggish if only a

small amount of Fe is available. This conclusion is in line with the observations of Rimsaite (1970), who also found that the breakdown process of mica is related to its Fe content. A higher Mg content may stabilize F known as F-Fe avoidance principle (recognized since Ramberg 1952), and also increase the stability of mica (e.g., Sanz and Stone 1979). This may be the reason why we observed  $T_2$  at higher temperatures, although the F content of these samples is still quite small and therefore the error on the analyses rather large.

In samples Berg 18, Uganda 1, and Pa1, a third temperature,  $T_3$ , may be distinguished around 1000 °C. In contrast to  $T_1$  and  $T_2$ , the EMF decreases at  $T_3$  ( $f_{O_2}$  increases). The temperature around 1000 °C compares well with the breakdown temperature of the final dehydroxylation (Eq. 3). Hogg and Meads (1975), looking at the Mössbauer effect in mica that was heated above 1000 °C for several hours, observed magnetic hyperfine interactions. These findings suggested the presence of  $\alpha$ -Fe<sub>2</sub>O<sub>3</sub> resulting from the breakdown of mica to oxides. In our case, there is no such indication, not even of superparamagnetism (Fig. 4). If mica breakdown was initiated at  $T_3$ , the duration of our EMF experiments at or above 1000 °C was too short to obtain detectable amounts of the breakdown products.

#### Effect of heating on biotite structure

Heating, however, did cause structural changes in the micas, as revealed by XRD and Mössbauer spectroscopy. Figure 6 compares the XRD pattern of sample Uganda 2 before (pristine) and after (used) the EMF experiment. The XRD pattern show four major features: no new phase(s) is present; the peak intensities increase although differentially; peak resolution decreases; and the unit-cell basal spacing decreases. We interpret these features to indicate that the heat treatment was too short for diffusion-controlled nucleation and growth of any additional phases. The differential changes in intensity of the basal reflections and the loss of  $\alpha$ -2 peak resolution from the pristine to used mica suggest structural changes within the K-containing or Fe,Mg containing planes. Sample preparation could have influenced orientation and hence intensities of mica diffraction, however, mica preparation was internally calibrated with cerium oxide and samples were not re-ground. Specifically, note that the (008) reflection at about 75° has a 1:1 ratio between used and

<sup>2</sup> Although we consider the reaction of OH<sup>-</sup> with the mica as the most likely explanation of our findings, the possibility cannot be ruled out that OH<sup>-</sup> migrates along the positive holes caused by defects of the Y-doping. This process has been considered earlier in relation to zirconia cells being able to sense the pH (e.g., Niedrach 1982; Bourcier et al. 1987). This pH sensing occurred, however, at temperatures below 300 °C, and was not enhanced with temperature. To initiate ZrO<sub>2</sub> to sense the pH, immersion in water for several hours to days was necessary. Our exposure times were short and not in high H<sub>2</sub>O or OH<sup>-</sup> concentration. Therefore, we do not believe that OH<sup>-</sup> migration in the ZrO<sub>2</sub> was involved in our experiments.

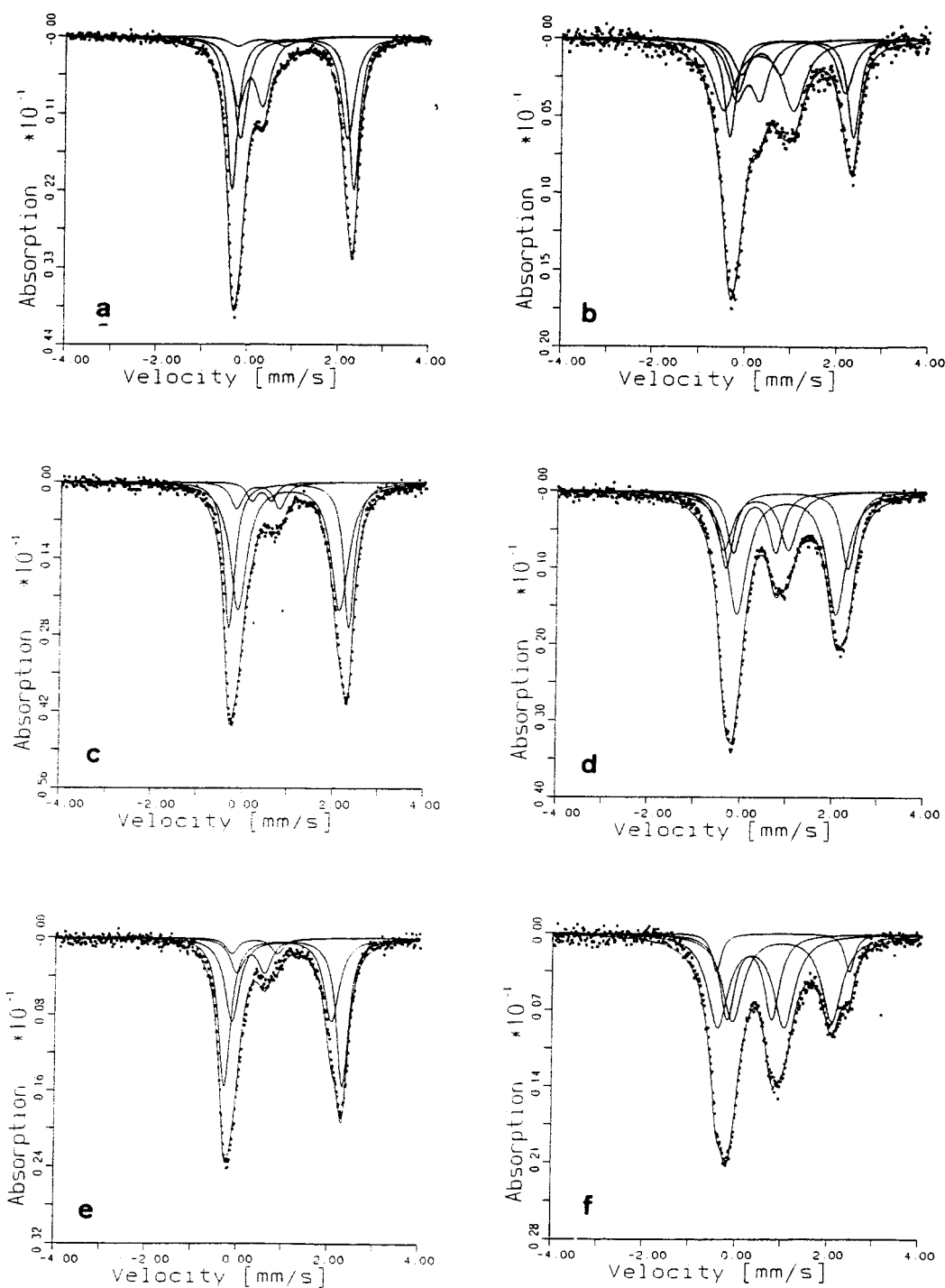


**FIGURE 4.** Mössbauer spectra of selected biotites prior to (a, c, e) and after (b, d, f) the EMF experiment. In all cases, the EMF experiment caused an increase of the line widths of the doublets, an increase of  $\text{Fe}^{3+}$  quadrupole splitting, and a small decrease of the  $\text{Fe}^{2+}$  quadrupole splitting. Specifically: (a) Biotite Pa2, prior to the experiment. Pa2 is an Al-undersaturated ferri-phlogopite and shows 22% of the total iron as  $^{57}\text{Fe}^{3+}$ . The concentration of  $^{57}\text{Fe}^{3+}$  is low; (b) Biotite Pa2, after the EMF experiment. The amount of  $^{57}\text{Fe}^{3+}$  has increased from 4 to 43% of

the total Fe; (c) Biotite Berg 11b prior to the EMF experiment. The spectrum is typical for biotite with a composition intermediate between annite and phlogopite, with 12%  $^{57}\text{Fe}^{3+}$ , and no evidence for  $^{57}\text{Fe}^{3+}$ ; (d) Biotite Berg11b after the EMF experiment. Twenty-one percent of  $\text{Fe}^{2+}$  was oxidized to  $\text{Fe}^{3+}$ ; (e) Biotite Berg3a prior to the EMF experiment is similar to Berg 11b but has a higher initial  $\text{Fe}^{3+}$  content of 18%; and (f) Biotite Berg3a after the EMF experiment shows an increase in  $\text{Fe}^{3+}$  by 59%.

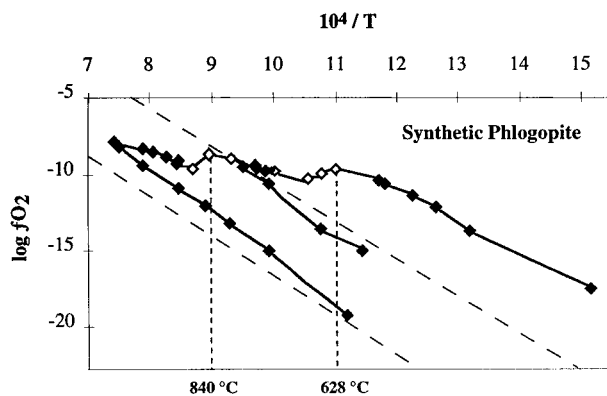


FIGURE 5. EMF pattern of a synthetic hydroxy-fluorophlogopite is of Type a.

pristine whereas the (005) reflection at about  $45^\circ$  has a 2:1 ratio. Inasmuch as these multiple reflections and the overall pattern have the same background, slurry sample preparation could not have produced these changes. These results support incipient change within the mica structure as a result of heat treatment.

In the Mössbauer spectra (Fig. 4, Table 3) the effect of heating on the local environment of Fe is seen in an increase of the line width of all doublets, except for that of  $\text{Fe}^{2+}$  at the octahedral M2 site of Berg 3a. This broadening of the resonant absorption lines is probably due to increasing imperfection of the coordination polyhedra and the lattice as a whole. The latter is probably caused by the oxidation of  $\text{Fe}^{2+}$  to  $\text{Fe}^{3+}$ . The quadrupole splitting,  $\Delta E_q$ , of  $\text{Fe}^{3+}$  on the octahedral M1 and M2 sites significantly increases by about 0.4 mm/s in all samples. This change is due to differences in local geometries of the anion and next-nearest neighbor cation arrangement around  $\text{Fe}^{3+}$ : the increase of  $\Delta E_q$  for  $\text{Fe}^{3+}$  indicates a more-distorted environment of octahedra in the oxidized mica. In a similar way, there is a less-pronounced decrease of  $\Delta E_q$  for  $\text{Fe}^{2+}$ , except for Berg 3a. The oxidized Berg 3a shows a very large  $\Delta E_q$  for  $\text{Fe}^{2+}$  of 2.92 mm/s on the M2 site and a rather small line width. Because this sample contains 59%  $\text{Fe}^{3+}$ , it is assumed that this doublet corresponds to another type of coordination, i.e., rearranged octahedron with only  $\text{O}^{2-}$  ions coordinating the  $\text{Fe}^{2+}$ . This means that during heating, less hydrogen is available to reduce the cell atmosphere within the  $\text{ZrO}_2$ . This lack of hydrogen might be another explanation for the shift of this sample to quite oxidized values in the  $1/T$ -log  $f_{\text{O}_2}$  diagram.

### CONCLUSIONS

The  $\text{ZrO}_2$  electrochemical technique provides reproducible signatures of Fe-bearing hydrous minerals, such as biotite, of steady-state and non-steady-state behavior in  $1/T$ -log  $f_{\text{O}_2}$  space. In the steady-state behavior (except for samples with carbon or adsorbed gases) data cluster within  $\pm 1$  log units of the FMQ buffer, in agreement with classical expectations for rocks containing mica. The non-

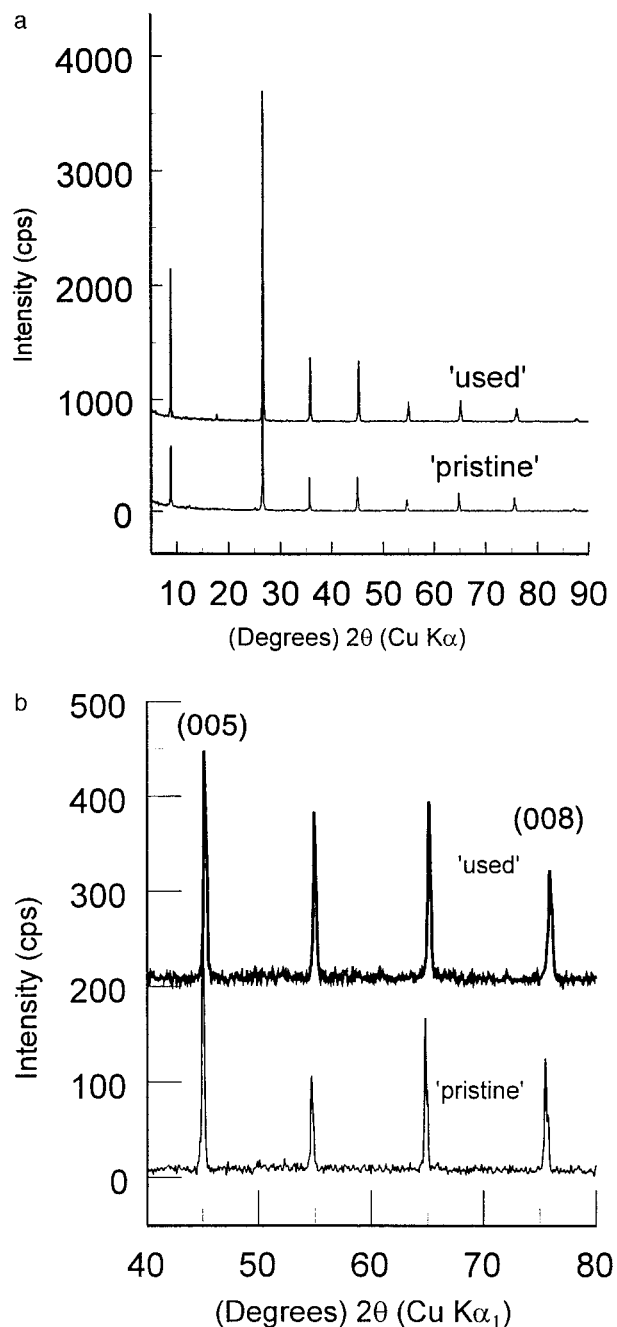


FIGURE 6. XRD patterns of the Uganda 2 mica before ("pristine") and after ("used")  $\text{ZrO}_2$  cell heat treatment. In a, the "used" pattern is shifted about 800 counts for clarity; in b, the "used" pattern is shifted about 800 counts and the  $2\theta$  axis is expanded for clarity.

steady-state behavior at temperatures  $T_1$ ,  $T_2$ , and  $T_3$ , detects three major breakdown events, anticipated in the literature: (1) liberation of surface-absorbed and loosely bonded  $\text{H}_2\text{O}$  and  $\text{CO}_2$  at temperatures below  $500^\circ\text{C}$ ; (2) the onset of oxidation, sometimes observable in up to three episodes, at  $505$  to  $546^\circ\text{C}$  ( $T_1$ ),  $680$  to  $890^\circ\text{C}$  ( $T_1$ ),

and around 880–890 °C for biotite, and 950 °C for phlogopite ( $T_2$ ); and (3) the onset of final dehydroxylation around 1000 °C ( $T_3$ ). Oxidation was confirmed by Mössbauer spectroscopy.

While we here propose a new application of the  $ZrO_2$ -EMF method, the qualitative approach, demonstrated could evolve in the future to characterize hydrous mineral breakdown signatures in relation to crystal chemistry. Employing constant, fixed heating rates might provide access to breakdown reactions, much like standard DTA or DSC patterns have been utilized to characterize, for example, clays (Mackenzie 1957, 1970). Such standardized patterns should be able to “fingerprint” hydrous minerals of different geologic settings.

### ACKNOWLEDGMENTS

We thank Aldo Cundari, University of Naples, who kindly provided the pyroxenite and phlogopite, C5691 and C5927 from Uganda, and we thank Bill Birch, Museum of Victoria, Melbourne, Australia, who offered three samples, Pa1 and Pa2 from Palabora and M4347 from the Vesuvius. A synthetic sample (Hatch et al. 1957) was supplied by William Kneller. The studies started in 1989 with some partial help of the Deutsche Forschungsgemeinschaft for D.J.M.B., which is acknowledged. D.J.M.B. thanks the University of Melbourne, Australia, for hospitality and access to their microprobe during the years 1988 through 1990. Temple University supplied precious metals,  $ZrO_2$ , and gases. A Humboldt Fellowship for G.C.U. (1992–1993) helped us to overcome geographic separation facilitating discussions. G.J.R. thanks G. Amthauer, University of Salzburg, for the possibility to use the Mössbauer equipment and W. Lottermoser for help and discussions concerning Mössbauer spectroscopy. Comments and suggestions of Koster van Groos, David Jenkins, Robert F. Dymek, Russell O. Colson, and two anonymous reviewers are appreciated.

### REFERENCES CITED

- Annersten, H. (1974) Mössbauer studies of natural biotites. *American Mineralogist*, 59, 143–151.
- Annersten, H., Devavarayan, S., Hægström, L., and Wäppling, R. (1974) Mössbauer study of synthetic ferriphlogopite  $KMg_3FeSi_3O_{10}(OH)_2$ . *Physics Status Solidi (b)* 48, K137–K138.
- Arculus, R.J. and Delano, J.W. (1980) Implications for the primitive atmosphere of the oxidation state of earth's upper mantle. *Nature*, 288, 72–74.
- Badwal, S.P.S., Bannister, M.J., and Garret, W.G. (1984) Low-temperature behavior of  $ZrO_2$  oxygen sensors. In N. Claussen, M. Rühle, and A. Heuer, Eds., *Advances in Ceramics*, 12, Science and technology of zirconia II, 598–606. The American Ceramic Society, Columbus, Ohio.
- Bagin, V.I., Gendler, T.S., Dainyak, L.G., and Kuz'min, R.N. (1980) Mössbauer, thermo-gravimetric, and X-ray study of cation ordering and high-temperature decomposition in biotite. *Clays and Clay Minerals*, 28, 188–196.
- Bartos, B., Freund, H.-J., Kühlenbeck, H., and Neumann, M. (1986) Adsorption and reaction of  $CO_2$  on metal surfaces. Detection of an intrinsic precursor dissociation. In M. Grunze and H. Kreuzer, Eds., *Kinetics of Interface Reaction*, p. 164–174. Springer Series in Surface Sciences, Berlin.
- Bourcier, W.L., Ulmer, G.C., and Barnes, H.L. (1987) Hydrothermal pH sensors of  $ZrO_2$ , Pd hydrides, and Ir oxides. In G.C. Ulmer and H.L. Barnes, Eds., *Hydrothermal Experimental Techniques*, p. 157–188. Wiley-Interscience Publications, New York.
- Burkhard, D.J.M. (1993) Biotite crystallization temperatures and redox states in granitic rocks as indicator for tectonic setting. *Geologie en Mijnbouw*, 79, 337–349.
- Burkhard, D.J.M. and Ulmer, G.C. (1995a) Kinetics and equilibria of redox systems at temperatures as low as 300°C. *Geochimica et Cosmochimica Acta*, 59, 1699–1714.
- (1995b) Dynamic tracking of mica breakdown reactions by electrochemical measurements. *Physics and Chemistry of Minerals*, 22, 507–510.
- Burkhard, D.J.M., Hanson, B., and Ulmer, G.C. (1991)  $ZrO_2$  oxygen sensors: an evaluation of behavior at temperatures as low as 300 °C. *Solid State Ionics*, 48, 333–339.
- Claussen, N., Rühle, M., and Heuer, A. (1984) *Advances in Ceramic Sciences and technology of zirconia II*, 842 p. The American Ceramic Society, Columbus, Ohio.
- Cygan, G., Chou, I., and Sherman, D.M. (1996) Reinvestigation of the annite-sanidine + magnetite +  $H_2$  reaction using  $f_{H_2}$ -sensor technique. *American Mineralogist*, 81, 475–484.
- Deines, P., Nafziger, R.H., Ulmer, G.C., and Woermann, E. (1974) Temperature-oxygen fugacity tables for selected gas mixtures in the system C-H-O at one atmosphere total pressure. *Bulletin of the earth and mineral sciences experimental station*, 88, Pennsylvania State University, Pennsylvania.
- Dyar, M.D. (1990) Mössbauer spectra of biotites from metapelites. *American Mineralogist*, 75, 656–666.
- Dyar, M.D. and Burns, R.G. (1986) Mössbauer data of trioctahedral micas. Evidence for tetrahedral  $Fe^{3+}$  and cation ordering. *American Mineralogist*, 72, 102–112.
- Elliott, W.C., Grandstaff, D.E., Ulmer, G.C., Buntin, T.J., and Gold, D.P. (1982) An intrinsic oxygen fugacity study of platinum-carbon associations in layered intrusions. *Economic Geology*, 77, 209–226.
- Ericson, T. and Wäppling, R. (1976) Texture effects in  $3/2$ – $1/2$  Mössbauer spectra. *Journal of Physics (Paris)* 12-C6, 719–723.
- Eugster, H.P. and Wones, D.R. (1962) Stability relations of the ferruginous biotite, annite. *Journal of Petrology*, 3, 82–125.
- Farmer, V.C., Russell, J.D., and McHardy, W.J. (1971) Evidence for loss of protons and octahedral iron from oxidized biotites and vermiculites. *Mineralogical Magazine*, 38, 121–137.
- Ferrow, E. (1987) Mössbauer and X-ray studies on the oxidation of annite and ferriannite. *Physics and Chemistry of Minerals*, 14, 270–275.
- Friel, J. and Ulmer, G.C. (1974) Oxygen fugacity geometry of the Oka complex. *American Mineralogist*, 59, 314–318.
- Hatch, R.A., Humphrey, R.A., Eitel, W., and Comeforo, J.E. (1957) Synthetic mica investigations IX: Review of progress from 1947 to 1955. Report investigations 5337, 79 p. U.S. Department of Interior, Bureau of Mines, Washington, D.C.
- Huebner, S. (1987) The use of gas mixtures at low pressure to specify oxygen and other fugacities of furnace atmospheres. In G.C. Ulmer and H.L. Barnes, Eds., *Hydrothermal experimental techniques*, p. 20–60. Wiley-Interscience Publications, New York.
- Huijsmans, J.P.P., van der Meulen, S.B., and Siewers, E.J. (1989) Membrane based thin-layered SOFC components. In G. With, R.A. Terpsta, and R. Metselaar, Eds., *Euro-ceramics*, vol. 3, 3626–3530. Elsevier, London.
- Hogg, C.S. and Meads, R.E. (1975) A Mössbauer study of thermal decomposition of biotites. *Mineralogical Magazine*, 40, 79–88.
- Knauth, L.P. and Epstein, S. (1982) The nature of water in hydrous silica. *American Mineralogist*, 67, 510–520.
- Kozul, J., Ulmer, G.C., and Hewins, R.H. (1988) Intrinsic oxygen fugacity measurements of some Allende Type B inclusions. *Geochimica et Cosmochimica Acta*, 52, 2707–2716.
- Lottermoser, W., Kaliba, P., and Forcher, K. (1992) MOESALZ—A computer program for Mössbauer analyses; personal communication exchange software.
- Mackenzie, R.C. (1957) *Differential thermal analyses of clays*. Central Press, Aberdeen, Scotland.
- Mackenzie R.C., Ed. (1970) *Differential thermal analysis*, vol. 1. Academic Press, London.
- Miyamoto, M. and Mikouchi, T. (1996) Platinum catalytic effect on oxygen fugacity of  $CO_2$ - $H_2$  gas mixtures measured with  $ZrO_2$  oxygen sensors at  $10^5$  Pa from 1300 to 700 °C. *Geochimica et Cosmochimica Acta*, 60, 2917–2920.
- Muse, S. and Soejima, S. (1983) A method of producing oxide sensing ceramics. European Patent no. 0-345-824-A1 granted to NGK Insulators, Ltd. and extended to Germany, France and England.
- Niedrach, L.W. (1982) Use of a high temperature pH sensor as a “pseudo-

- reference electrode" in the monitoring of corrosion and redox potentials at 285°C. *Journal of the Electrochemical Society*, 212, 672–684.
- O'Neill, H.S. and Pownceby, M.I. (1993) Thermodynamic data from redox reactions at high temperatures: I. An experimental and theoretical assessment of the electrochemical method using stabilized zirconia electrolytes, with revised values for the Fe–FeO, Co–CoO, Ni–NiO and Cu–Cu<sub>2</sub>O oxygen buffers, and new data for the W–WO<sub>2</sub> buffer. *Contributions to Mineralogy and Petrology*, 114, 296–314.
- Ramberg, H. (1952) Chemical bonds and the distribution of cations in silicates. *Journal of Geology*, 60, 331–355.
- Rancourt, D.G. (1994a) Mössbauer spectroscopy of minerals I. Inadequacy of Lorentzian-line doublets in fitting spectra arising from quadrupole splitting distributions. *Physics and Chemistry of Minerals*, 21, 244–249.
- (1994b) Mössbauer spectra of mineral II. Problem of resolving cis and trans octahedral Fe<sup>2+</sup> sites. *Physics and Chemistry of Minerals*, 21, 250–257.
- Rancourt, D.G., Tume, P., and Lalonde, A.E. (1993) Kinetics of the Fe<sup>2+</sup> + OH<sup>-</sup> → (Fe<sup>3+</sup> + O<sup>2-</sup>)<sub>mica</sub> + H. Oxidation reaction in bulk single-crystal biotite studied by Mössbauer spectroscopy. *Physics and Chemistry of Minerals*, 20, 276–284.
- Rancourt, D.G., Christie, I.A.D., Royer, M., Kodama, H., Robert, J.L., Lalonde, A.E., and Murad, E. (1994a) Determination of accurate <sup>57</sup>Fe<sup>3+</sup>, <sup>57</sup>Fe<sup>2+</sup>, and <sup>57</sup>Fe<sup>2+</sup> site populations in synthetic annite by Mössbauer spectroscopy. *American Mineralogist*, 79, 51–62.
- Rancourt, D.G., Ping, J.Y., and Berman, R.G. (1994b) Mössbauer spectroscopy of mineral III. Octahedral-site Fe<sup>2+</sup> quadrupole splitting distribution in the phlogopite-annite series. *Physics and Chemistry of Minerals*, 21, 258–267.
- Redhammer, G.J., Beran, A., Dachs, E., and Amthauer, G. (1993) A Mössbauer and X-ray diffraction study of annites synthesized at different oxygen fugacities and crystal chemical implications. *Physics and Chemistry of Minerals*, 20, 382–394.
- Redhammer, G.J., Dachs, E., and Amthauer, G. (1995) A Mössbauer and X-ray powder diffraction studies of synthetic micas on the join annite K(Fe<sub>2</sub>AlSi<sub>3</sub>O<sub>2</sub>(OH)<sub>2</sub>-phlogopite K(Mg<sub>2</sub>AlSi<sub>3</sub>O<sub>2</sub>(OH)<sub>2</sub>). *Physics and Chemistry of Minerals*, 22, 282–293.
- Rimsaite, J. (1970) Structural formulae of oxidized and hydroxyl-deficient micas and decomposition of the hydroxyl group. *Contributions to Mineralogy and Petrology*, 25, 225–240.
- Rinne, F. (1924) Bemerkungen über strukturchemische Silikatformeln und den kristallographisch-chemischen Ab- und Umbau von Glimmer durch Entwässerung, Oxidation und Reduktion. *Akademische Wissenschaften Leipzig. Verhandlung*, 76, 1–11.
- Ross, G.J. and Rich, C.I. (1974) Effect of oxidation and reduction on potassium exchange of biotite. *Clays and Clay Minerals*, 22, 355–360.
- Sanz, J. and Stone, W.E.E. (1979) NMR study of micas, II. Distribution of Fe<sup>2+</sup>, F<sup>-</sup>, and OH<sup>-</sup> in the octahedral sheet of phlogopites. *American Mineralogist*, 64, 119–126.
- Sanz, J., Gonzalez-Careno, T., and Gancedo, R. (1983) On dehydroxylation mechanisms of biotite in vacuo and in oxygen. *Physics and Chemistry of Minerals*, 9, 14–18.
- Sato, M. (1965) Electrochemical geometry; a possible new method of geothermometry with electroconductive minerals. *Economic Geology*, 60, 812–818.
- (1971) Electrochemical measurements and control of oxygen fugacity and other gaseous fugacities with solid electrolyte sensors. In G.C. Ulmer, Ed., *Research techniques for high pressure and high temperature*, p. 43–99. Springer, New York.
- (1972) Intrinsic oxygen fugacities of iron-bearing oxide and silicate minerals under low total pressure. *Geological Society of America, Memoir*, 135, 279–306.
- Sato, M. and Valenza, M. (1980) Oxygen fugacities of the layered series of the Skaergaard intrusion, east Greenland. *American Journal of Science*, 280A, 134–158.
- Tripathi, R.P., Chandra, U., Chandra, R., and Lokanathan, S. (1978) A Mössbauer study of the effect of heating biotite, phlogopite and vermiculite. *Journal of inorganic nuclear chemistry*, 40, 1293–1298.
- Ulmer, G.C. (1984) ZrO<sub>2</sub> oxygen and hydrogen sensors: a geologic perspective. In *Advanced Ceramics 12, Science and Technology of Zirconia II*, p. 660–671. American Ceramic Society.
- Ulmer, G.C., Rosenhauer, M., Woermann, E., Ginder, J., Drory-Wolff, A., and Wasilewski, P. (1976) Applicability of electrochemical oxygen fugacity measurements to geothermometry. *American Mineralogist*, 61, 661–670.
- Ulmer, G.C., Grandstaff, D.E., Weiss, D., Moats, M., Buntin, T.J., Gold, D.P., Hatton, C.J., Kadik, A., Koseluk, R.A., and Rosenhauer, M. (1987) The mantle redox state; an unfinished story? *Geological Society of America, Special Papers*, 215, 5–23.
- Vedder, W. and Wilkins, R.W.T. (1969) Dehydroxylation and rehydroxylation, oxidation and reduction of micas. *American Mineralogist*, 54, 482–509.
- Veith, J.A. and Jackson, M.L. (1974) Iron oxidation and reduction effects on structural hydroxyl and layer charge in aqueous suspensions of micaeous vermiculites. *Clays and Clay Minerals*, 22, 345–353.
- Virgo, D., Luth, R.W., Moats, M., and Ulmer, G.C. (1988) Constraints on the oxidation state of the mantle: an electrochemical and <sup>57</sup>Fe Mössbauer study of mantle-derived ilmenites. *Geochimica et Cosmochimica Acta*, 52, 1781–1794.
- Wones, D.R. and Eugster, H.P. (1965) Stability of biotite: experiment, theory, and application. *American Mineralogist*, 50, 1228–1269.
- Yoder, H.S. and Eugster, H.P. (1954) Phlogopite synthesis and stability range. *Geochimica et Cosmochimica Acta*, 6, 157–185.

MANUSCRIPT RECEIVED JULY 9, 1998

MANUSCRIPT ACCEPTED SEPTEMBER 26, 1998

PAPER HANDLED BY ROBERT F. DYMEK